LONG–TERM INFLUENCE OF CONCRETE DEGRADATION ON DAM–FOUNDATION INTERACTION

Article *in* International Journal of Computational Methods · November 2011

DOI: 10.1142/S0219876211002472

4 authors, including:

A. Burman
National Institute of Technology Patna
21 PUBLICATIONS **142** CITATIONS

SEE PROFILE

Damodar Maity
Indian Institute of Technology Kharagpur
102 PUBLICATIONS **1,623** CITATIONS

SEE PROFILE

Sreedeep Sekharan
Indian Institute of Technology Guwahati
185 PUBLICATIONS **1,360** CITATIONS

SEE PROFILE

International Journal of

COMPUTATIONAL METHODS

Volume 8 • Number 3 • September 2011

Long-Term Influence of Concrete Degradation on Dam–Foundation Interaction

A. Burman, D. Maity, S. Sreedeep and I. Gogoi

World Scientific

NEW JERSEY • LONDON • SINGAPORE • BEIJING • SHANGHAI • HONG KONG • TAIPEI • CHENNAI

International Journal of Computational Methods
Vol. 8, No. 3 (2011) 397–423

DOI: 10.1142/S0219876211002472

World Scientific
www.worldscientific.com

LONG-TERM INFLUENCE OF CONCRETE DEGRADATION ON DAM–FOUNDATION INTERACTION

A. BURMAN*, D. MAITY†, S. SREEDEEP‡ and I. GOGOI§

*Lecturer, Department of Civil Engineering
BIT Mesra, Ranchi – 835215, India
avijit@iitg.ernet.in

†Associate Professor, Department of Civil Engineering
IIT Kharagpur, Kharagpur – 721302, India
dmaity@civil.iitkgp.ernet.in

‡Assistant Professor, Department of Civil Engineering
IIT Guwahati, Guwahati – 781039, India
srees@iitg.ernet.in

§Assistant Professor, Department of Civil Engineering
NIT Surathkal, Mangalore – 575025, India
indarnigogoi@yahoo.com

Received 23 December 2009
Accepted 4 June 2010

The dam–foundation interaction behavior under the application of seismic load has been investigated in the present paper using finite element technique in the time domain. Since the dam face is in constant contact with water, concrete degradation due to hygromechanical loading is inevitable and should be considered in the analysis procedure. This ageing process of concrete leads to loss of stiffness and strength of the material. Therefore, to assess the behavior of the dam at a later stage of its life, it is important to determine the proper strength of the concrete at a certain age. An approach to include the time-dependent degradation of concrete owing to environmental factors and mechanical loading in terms of isotropic degradation index is presented. An iterative scheme has been developed to model the dam–foundation interaction effects of the coupled system. The strains and the displacements are observed to increase if the ageing procedure of the gravity dam is taken into account. The long-term behavior of the aged concrete gravity and foundation interaction has been observed by using a developed ageing model for concrete.

Keywords: Concrete gravity dam; material degradation; iterative scheme; isotropic degradation index; dam–foundation interaction.

1. Introduction

The issues of seismic safety of dams have been looked at with increased attention in various parts of the world in recent years. Considerable research has been conducted

*Corresponding author.

in the area of dynamic interaction analysis of dam–foundation coupled system. An excellent amount of work on dam–reservoir–foundation interaction in the frequency domain or indirect time domain has been carried out by Chopra and his colleagues [Chopra and Chakrabarty (1981); Fenves and Chopra (1985)].

Since the dam–foundation interaction problem requires modeling of semi-infinite foundation domain, it is necessary to impose proper nonreflecting boundary conditions (NRBCs) at the truncated boundary, so that the traveling waves are not reflected back in the foundation domain. There are two main types of NRBCs: *approximate local* NRBCs and *exact nonlocal* NRBCs. Most of the NRBCs belong to the former category. The first local boundary or the first transmitting boundary is proposed by Lysmer and Kuhlemeyer [1969]. It is also known as viscous or absorbing boundary since it places viscous dashpots at the boundary to absorb the energy of the traveling waves. An example of nonlocal NRBC is the boundary conditions proposed by Grote and Keller [1996], which are further modified by Thompson and Huan [2000] to improve the scaling of the related first-order equations. Boundary element method is a powerful method for modeling the semi-infinite soil medium since only the boundaries of the unbounded medium are discretized so that the spatial dimension is reduced by one and the radiation condition is satisfied automatically as a part of the fundamental solution. Based on the substructure method, Zienkiewicz *et al.* [1977] and Estorff and Kausel [1989] suggested many coupled FEM–BEM methods where the structure and the adjacent finite region of soil are discretized by the standard finite element method while the unbounded soil is modeled by the boundary element method. However, it is not very easy to derive the fundamental solutions for many types of problems. Wolf and Song [1996] developed the scaled boundary element method (also known as consistent infinitesimal finite element cell method) by combining the advantages of the boundary element method and the finite element method. This method is exact in radial direction and converges to the exact solution in the finite element sense in the circumferential direction, and is rigorous in space and time.

Felippa and Park [1980] discussed, in details, staggered solution procedure for the solution of a variety of coupled field dynamic problems. Direct solution methods of coupled field problems suffer from the need of excessive storage requirements and computation time. The staggered solution schemes allow us to use reduced matrices for the particular subsystem leading to less time for solution. Rizos and Wang [2002] developed a partitioned method for soil–structure interaction analysis in the time domain through a staggered solution method using both FEM and BEM. Maity and Bhattacharyya [2003] suggested an iterative scheme in conjunction with the staggered solution procedure for the dam–reservoir interaction problems. According to Estorff and Hagen [2005], the staggered approach should be used with great care, since its stability is conditional on the size of time step. If a corrective iteration at each time step is employed, where the interface boundary conditions are iteratively updated until convergence is achieved, one obtains an iterative coupling method. Within the iteration procedure at every time step, a relaxation operator

may be applied to the interface boundary conditions in order to enable or speed up convergence. Jahromi *et al.* [2007] used partitioned analysis technique involving iterative coupling procedure for solving different soil–structure interaction problems.

For a more realistic estimation of the dynamic behavior of an existing or a new dam at any age, it is important to estimate the material degradation with ageing, so that the stiffness of the dam can be accurately determined. At an early age, the rate of strength gain is faster but the rate is reduced with age. It is customary to assume the 28-day strength as the full strength of concrete, but experimental evidences [Washa *et al.* (1989)] show that concrete develops strength beyond 28 days. Though various nonlinear analysis procedures have been developed to determine the effect of damage on the responses of the dam due to seismic excitation, primary mechanisms or factors that can produce premature deterioration of concrete dams need to be identified. Ulm and Coussy [1995] explored the theory of reactive porous media for modeling of concrete at early ages. The model accounts explicitly for hydration of cement by considering the thermodynamic imbalance between the chemical constituents. Bazant *et al.* [1997] proposed a new physical theory and constitutive model considering effects of long-term ageing and drying on concrete creep. Bazant and Xiang [1997] proposed a solution procedure to predict the design lifetime of concrete considering crack growth and long-time loading. Some researchers [Ghaemian and Ghobarah (1999)] had considered the dam–reservoir interaction problem with an isotropic damage while developing a nonlinear damage model. The damage index used in the above procedures is mainly evaluated based on relation between the strain energy of the damaged material and elastic energy of the undamaged material. A coupled hygromechanical model for finite-element analyses of structures made of partially saturated porous media consisting of cementitious materials such as concrete was formulated by Meschke and Grasberger [2003]. Cervera *et al.* [1999 a,b; 2000 a,b] proposed a thermochemical model to simulate the hydration and ageing process of concrete considering creep and damage in a roller compacted concrete dam. The evolution of temperature, elastic moduli, and compressive and tensile stress distributions inside the dam can be predicted in terms of amount of ageing at any time during the construction process and also during the years following the completion of the dam. This procedure can be applied to understand the effect of some major variables such as the placing temperature, the starting date, and the placing speed on the construction process. In the long-term, ageing of concrete is affected by the concentration of various constituents in the concrete matrix, chemical reactions such as calcium leaching or alkali–silica reaction (ASR), moisture transport, and loading due to submergence in water. According to Cervera *et al.* [2000b], the consideration of creep is significant if the stress analysis includes simulation of construction process. The model describes the behavior of early age concrete. Bangert *et al.* [2003] evaluated the long-term material degradation in concrete structures due to a chemically induced degradation processes and calcium leaching. Steffens *et al.* [2003] introduced an ageing approach to determine the degradation of concrete structures considering water effect on ASR.

A comprehensive mechanical model was proposed for the material swelling with a hydrochemomechanical approach, to study structural effects of ASR.

In this paper, a time domain staggered solution approaches with iterative scheme has been used to solve dynamic dam–foundation interaction problems. This method performs all the calculations in time domain in contrast to the most of the substructure techniques. The substructure techniques, while computing the interaction forces require applying Fourier transformations and then evaluating the convolution integrals that are computationally very demanding and complex processes [Wolf (1985)]. It does not require calculation of the free field motion of the foundation as is required by the substructure method and all the calculations are performed in terms of the absolute displacements. The advantage of this staggered solution procedure is that there is no need to calculate the coupled mass, damping, and stiffness matrices that appear in direct coupling equations of interaction problems. The soil and structure domain are solved sequentially and the interaction is enforced by the proposed iterative method. In order to represent the infinite nature of the foundation domain, viscous dashpots as suggested by Lysmer and Kuhlemeyer [1969] has been adopted and its performance has been observed. A parameter called the degradation index is used in the analysis to account for the extent of isotropic degradation occurring in the concrete. The degradation index within the elastic limit is derived considering factors due to exposure of concrete to water, mechanical loading, and chemical reaction, etc. Thus, the response of the concrete gravity dam at various ages after construction has been simulated in the present work taking into account of the effect of dam–foundation interaction effects.

2. Modeling of Aged Concrete Dam

The dam has a long body whose geometry and loading conditions do not vary in the longitudinal direction. Therefore, the dam structure can be analyzed under plane strain idealization. Therefore, the constitutive relation for elastic isotropic material can be written as

$$\{\sigma\} = [D]\{\varepsilon\}. \tag{1}$$

In the above equation, $\{\sigma\}^{\mathrm{T}} = \{\sigma_x, \sigma_y, \tau_{xy}\}$ and $\{\varepsilon\}^{\mathrm{T}} = \{\varepsilon_x, \varepsilon_y, \gamma_{xy}\}$ are the vectors of stress and strain respectively, and $[D]$ is the constitutive matrix defined as

$$[D] = \frac{E_d}{(1+\mu)(1-2\mu)} \begin{bmatrix} (1-\mu) & \mu & 0 \\ \mu & (1-\mu) & 0 \\ 0 & 0 & \dfrac{(1-2\mu)}{2} \end{bmatrix} \tag{2}$$

for a material with elastic modulus E_d and Poisson's ratio μ. The concept of degradation of concrete strength is based on the reduction of the net area capable of supporting stresses. Adopting an analogy given by Ghrib and Tinawi [1995] to

measure the extent of damage in concrete, the orthotropic degradation index can be determined as

$$d_{gi} = 1 - \frac{\Omega_i - \Omega_i^d}{\Omega_i} = 1 - \frac{\Omega_i^n}{\Omega_i}. \tag{3}$$

Here, Ω_i is the tributary area of the surface in direction i and Ω_i^d is the area affected by degradation. In a scale of 0 to 1, the orthotropic degradation index, $d_{gi} = 0$ indicates no degradation and $d_{gi} = 1$ indicates completely degraded material. The index $i = 1, 2$ corresponds with the Cartesian axes x and y in two-dimensional (2D) case. The effective plane strain material matrix can be expressed as

$$[D_d] = \frac{E_d}{(1+\mu)(1-2\mu)} \begin{bmatrix} (1-\mu)\Lambda_1^2 & \mu\Lambda_1\Lambda_2 & 0 \\ \mu\Lambda_1\Lambda_2 & (1-\mu)\Lambda_2^2 & 0 \\ 0 & 0 & (1-2\mu)\Lambda_1^2\Lambda_2^2/(\Lambda_1^2+\Lambda_2^2) \end{bmatrix}, \tag{4}$$

where Λ_1 is $(1 - d_{g1})$ and Λ_2 is $(1 - d_{g2})$. In the above equation, E_d is the elastic modulus of the material without degradation. If $d_{g1} = d_{g2} = d_g$, the isotropic degradation model is expressed as

$$[D_d] = (1 - d_g)^2[D], \tag{5}$$

where $[D_d]$ and $[D]$ are the constitutive matrices of the degraded and undegraded model, respectively.

2.1. *Evaluation of degradation index*

The compressive strength of concrete is expected to decrease with age due to chemical and mechanical material degradations. However, it is also a known fact that concrete gains compressive strength with age. In the present work, an attempt is made to simulate the concrete strength considering both of these above-mentioned factors.

To consider the detrimental effect of chemical and mechanical material degradations, the total porosity of concrete is taken as a measure to determine the degradation parameter. The total porosity, ϕ, is defined as the sum of the initial porosity, ϕ_0, the porosity due to matrix dissolution, ϕ_c, and the apparent mechanical porosity, ϕ_m. Bangert *et al.* [2003] and Kuhl *et al.* [2004] have outlined the detailed procedure of calculating mechanically induced porosity, which is as follows:

$$\phi = \phi_0 + \phi_c + \phi_m. \tag{6}$$

The apparent mechanically induced porosity, ϕ_m, considers the influence of mechanically induced micropores and microcracks on the macroscopic material properties of the porous material. According to Bangert *et al.* [2003], it is obtained as

$$\phi_m = [1 - \phi_0 - \phi_c]d_m, \tag{7}$$

where d_m is the scalar degradation parameter. The strain-based exponential degradation parameter as proposed by Gogoi and Maity [2007] may be expressed as

$$d_m = a_s - \frac{\kappa^0}{\kappa}[1 - \alpha_c + \alpha_c e^{(\beta_c[\kappa^0 - \kappa])}], \tag{8}$$

where κ^0 and κ are values of strain that represents the initial threshold degradation and the internal variable defining the current damage threshold depending on the loading history. The parameter κ^0 is given by f_t/E_0, where f_t is the static tensile strength and E_0 is the elastic modulus of the undegraded material before any mechanical loading is imposed. The value of d_m at any age can be determined from Eq. (8) that will vary with κ caused by the mechanical loading history. Here, α_c and β_c are material parameters that can be obtained experimentally [Bangert *et al.* (2003)]. In Eq. (8), the value of a_s is considered to be 1.0 by Simo and Ju [1987], which is the maximum allowable degradation due to mechanically induced porosity.

Atkin [1994] described that the ageing process may be described by a normalized process extent with $\varsigma = 0$ for a freshly laid concrete and $\varsigma = 1$ for its completely aged state. Thus, the kinetic law for the ageing process may be stated as

$$\dot{\varsigma} = \frac{1}{\tau_a}(1 - \varsigma)_m, \tag{9}$$

where $\dot{\varsigma}$ is the time derivative of ς and τ_a is the characteristic time of the ageing process, which can be assumed to be the design life of the structure. Integrating Eq. (9) with respect to time, the following expressions will be obtained:

$$1 - \varsigma = e^{(-\frac{t}{\tau_a})}. \tag{10}$$

Replacing ς with degradation index d_g in Eq. (10), variation of degradation index with time can be given as

$$d_g = 1 - e^{(-\frac{t}{\tau_a})}. \tag{11}$$

The hygrochemomechanical approach to describe the aging of concrete involves modeling of amorphous gel, aging water combination process, and chemomechanical material swelling. The amorphous gel and the chemomechanical swelling lead to the formation of porosity in concrete which in turn reduces its strength. The detailed description of the gel formation and other mechanisms are well described in the work of Steffens *et al.* [2003]. As a first approximation, the gel formation process is described by a parameter called reaction extent $\xi_\gamma \in [0, 1]$ with $\xi_\gamma = 0$ for the beginning of the reaction and $\xi_\gamma = 1$ for the end of the reaction. Steffens *et al.* [2003] suggested the value reaction extent, ξ_γ, for the corresponding characteristic time, τ_r, at a constant ambient humidity and is given by

$$\xi_\gamma = 1 - e^{(-\frac{t}{\tau_r})}. \tag{12}$$

Substituting t from Eq. (11) in Eq. (12), we can arrive at the following relation,

$$1 - d_g = (1 - \xi_\gamma)^{\frac{\tau_r}{\tau_a}}. \tag{13}$$

The relation between degraded elastic modulus due to porosity of concrete, E_n, and the elastic modulus of concrete considering strength gain at a particular age, E_0, can be given as $E_n = (1 - d_g)E_0$. Using the dimensionless value of total porosity obtained by multiplying the scalar degradation variable, as reaction extent, the variation of degradation with respect to time can be given as

$$E_n = (1 - \phi)^{\frac{t_a}{\tau_a}} E_0. \tag{14}$$

The value of τ_a is the characteristic age for which the structure is designed and t_a is the time corresponding to which the degradation index is determined. Once the value of degraded elastic modulus is obtained from Eq. (14), the isotropic degradation index, d_g, can be determined as

$$d_g = 1 - \frac{E_n}{E_0}. \tag{15}$$

2.2. *Gain in compressive strength with age*

It is a known fact that concrete gains compressive strength with age. This phenomenon is predicted by a curve fitting on 50 years of compressive strength data published by Washa *et al.* [1989]. The compressive strength test results of various concrete specimens of different proportions were published in the referred literature. These specimens were cured for 28 days and then placed in outdoors, which was on level ground in an open location. All the specimens were kept in open, so that they were subjected to change in severe weather conditions of 25 cycles of freezing and thawing each winter, annual precipitation including snowfall of about 0.813 cm, and air temperature variation between $-32.0°$C and $35.0°$C.

A least square curve fitting analysis is attempted on the set of compressive strength data published by Washa *et al.* [1989]. In engineering problems, an experiment produces a set of data points $(x_1, y_1), \ldots, (x_n, y_n)$, where the abscissas $\{x_k\}$ are distinct. While choosing the particular mathematical function for the curve fitting of the experimental data sets, it should be kept in mind that the mathematical function should be comprised of physically meaningful parameters. In the present case, we seek to suggest a mathematical function involving the time in years and the compressive strength of concrete. While expressing these experimental data by a mathematical function of the form $y = f(x)$, some errors are inevitable because of test conditions of the experiments or any other types of errors. Therefore, the actual value $f(x_k)$ [Mathews (2001)] satisfies

$$f(x_k) = y_k + e_k, \tag{16}$$

where e_k is the measured error. Some of the methods that can determine how far the curve $y_{ls} = f(x)$ lies from the data are:

$$\left.\begin{aligned} &\text{Maximum error} : E_\infty(f) = \max_{1\le k\le N'}\{|f(x_k) - y_k|\} \\ &\text{Average error} : E_1(f) = \frac{1}{N'}\sum_{k=1}^{N'}|f(x_k) - y_k| \\ &\text{Root-mean-square error} : E_2(f) = \left[\frac{1}{N'}\sum_{k=1}^{N'}|f(x_k) - y_k|^2\right]^{1/2} \end{aligned}\right\}. \tag{17}$$

The *best fitting* line is found by minimizing one of the quantities in Eq. (17). Among a all the three choices given in Eq. (17), $E_2(f)$ is preferred most of the times because of computational convenience. The *least squares line* is the line that minimizes the root-mean-square error $E_2(f)$ and is given as

$$y_{ls} = f(x) = Ax + B. \tag{18}$$

In Eq. (18), A and B can be determined from N' sets of experimental data as follows:

$$A = \frac{\sum_{k=1}^{N'} x_k y_k}{\sum_{k=1}^{N'} x_k}, \quad B = \frac{\sum_{k=1}^{N'} y_k}{N'} - A\frac{\sum_{k=1}^{N'} x_k}{N'}. \tag{19}$$

For the present work, the 50 years of compressive strength data set corresponds to a concrete specimen of mixed proportion 1 : 2.51 : 5.34 (cement: sand: gravel by weight) with water cement ratio of 0.49. Here, the following forms are considered for curve fitting:

$$\text{I.} \quad y = C'x^A. \tag{20}$$

In the above expression, $C' = e^B$ and $D' = -A$. Data linearization is carried out by transforming points (x_k, y_k) in the xy plane by the operation $(X_k, Y_k) = (\ln(x_k), \ln(y_k))$ in the XY plane for curve I. Then, the least squares line is fitted to the points $\{(X_k, Y_k)\}$ to give the predicted results. The predicted results using the above expressions (20) are plotted in Fig. 1. It is observed from Fig. 1 that curve I also shows excellent agreement with the experimental data of 50 years of concrete compressive strength. Therefore, it is concluded that an equation in the form of curve I may be used to predict the evolution of compressive strength of concrete over time. The equation is as follows:

$$f(t) = 43.47t^{0.08}. \tag{21}$$

Equation (21) has been obtained by carrying out a least square analysis using a curve of the form $y = C'x^A$ with the necessary transformation of the coordinates as mentioned before. In this case also, the values of C and A obtained are 43.47 and 0.08, respectively. Having obtained the value of compressive strength of concrete at

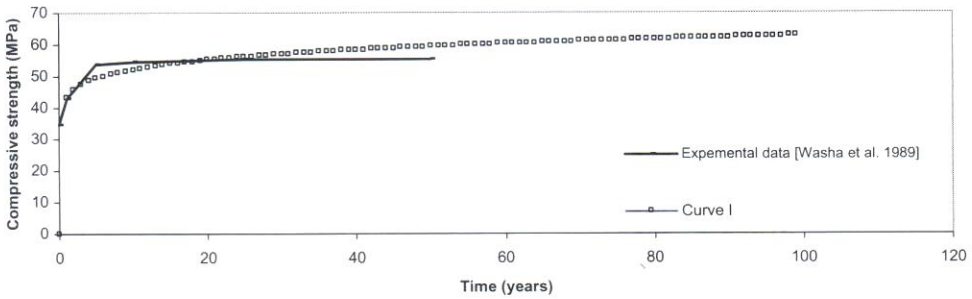

Fig. 1. Curve fitting of experimental data.

a certain age, the value of static elastic modulus of concrete in SI units [Neville and Brooks (1987)] is calculated from

$$E_0 = 4733\sqrt{f(t)}. \tag{22}$$

After calculating the static elastic modulus of concrete, E_0, the degraded elastic modulus of concrete (E_n) due to various hygrochemomechanical effects may be obtained from Eq. (14). Having obtained the value of E_n, the value of degradation index is given by Eq. (15) [Gogoi and Maity (2007)].

3. Modeling of the Foundation Domain

In the present work, the foundation material is assumed to be of rock in nature. A linear elastic constitutive model has been chosen to simulate the stress vs. strain behavior of soil. Equation (2) has been used to represent the constitutive behavior of the rock material.

4. Calculation of Hydrodynamic Pressure

Figure 2 describes the geometry of dam and adjacent reservoir. Assuming the reservoir water to be inviscid and incompressible and its motion to be of small amplitude, the governing equation for hydrodynamic pressure is as follows [Westergaard (1933)]:

$$\nabla^2 p = 0. \tag{23}$$

Here, $\nabla^2 = (\partial^2/\partial x^2) + (\partial^2/\partial y^2)$ and is called the Laplacian operator and p is the hydrodynamic pressure. The solution of Laplace equation can be expressed in Eq. (24) with the following assumptions:

(i) The bottom of the fluid domain is horizontal and rigid.
(ii) The fluid–structure interface is vertical.

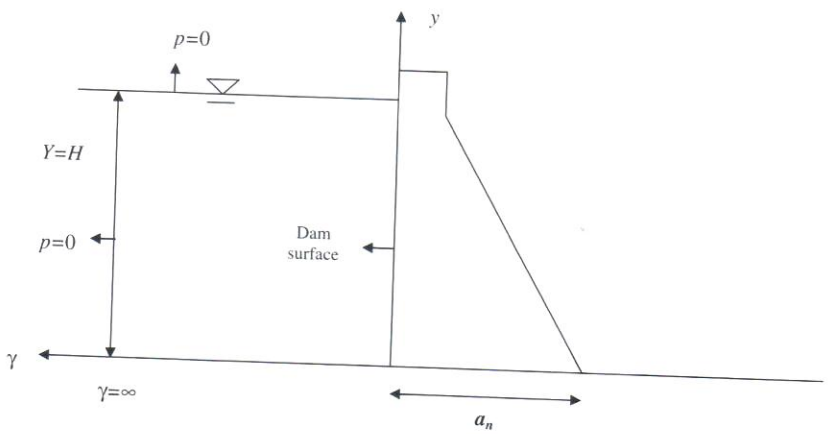

Fig. 2. Geometry of the reservoir domain.

(iii) The fluid domain extends to infinity and its motion is two dimensional.

$$p = 2a_n \rho H \sum_{n=1}^{\infty} \frac{(-1)^{n+1}}{\lambda_n^2} e^{(-\lambda_n \frac{x}{H})} \cos\left(\lambda_n \frac{y}{H}\right), \tag{24}$$

where p = hydrodynamic pressure at the upstream face of the dam; a_n = the magnitude of acceleration normal to the upstream face of the dam; ρ = the mass density of water; H = The height of water at the upstream side of the dam; and y = the variation of distance in the vertical direction.
Where,

$$\lambda_n = \frac{(2n-1)\pi}{2}. \tag{25}$$

The hydrodynamic pressure on the dam has been calculated using Eq. (24).

5. Viscous or Absorbing Boundary

A way to eliminate waves propagating outward from the structure is to use Lysmer boundaries. This method consists of simply connecting dashpots to all degrees of freedom of the boundary nodes and fixing them on the other end (Fig. 3). Lysmer boundaries are derived for an elastic wave propagation problem in a 1D semi-infinite bar. The damping coefficient C of the dashpot equals

$$C = A\rho c, \tag{26}$$

where A is the section of the bar, ρ is the mass density, and c the wave velocity that has to be selected according to the type of wave that has to be absorbed (shear wave velocity C_s or compressional wave velocity C_p). In two dimensions, Eq. (26) takes the following form, which results in dampers coefficients C_n and C_t in the

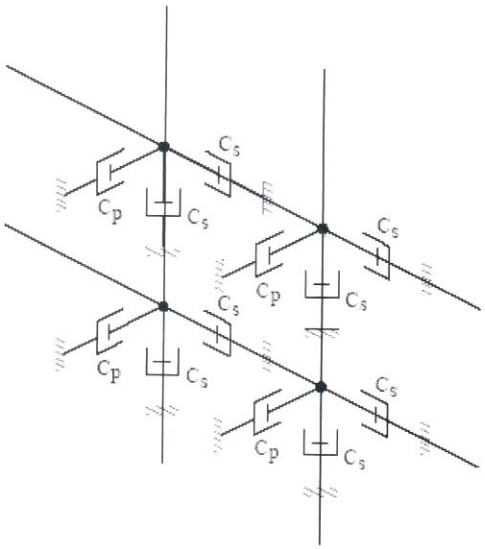

Fig. 3. Viscous dashpots connected to each degrees of freedom of a boundary node.

normal and tangential directions.

$$C_n = A_1 \rho c_p \tag{27}$$

$$C_t = A_2 \rho c_s. \tag{28}$$

The dashpot coefficients, c_s and c_p, in two mutually orthogonal directions are given by the following expressions: the shear wave velocity C_s and compressional wave velocity C_p are given by

$$C_s = \sqrt{\frac{G}{\rho}} \tag{29}$$

$$C_p = \sqrt{\frac{E(1-\nu)}{(1+\nu)(1-2\nu)\rho}}, \tag{30}$$

where G is the shear modulus of the medium and is expressed as

$$G = \frac{E}{2(1+\mu)}. \tag{31}$$

Here, E is the Young's modulus and μ is the Poisson's ratio. This procedure leads to the frequency-independent boundary conditions that are local in time and space. If the shape functions of the neighboring finite elements are used instead of crude lumping procedure, a narrow-banded damping matrix arises, which is also easy to implement.

However, in general, the directions of the incident waves are not known in advance. In these cases, it may be advantageous to use a "diffused" version of

expressions (27) and (28) as suggested by White *et al.* [1977]. Assuming that wave energy arrives at the boundary with equal probability from all directions, effective factors A_1 and A_2 are evaluated by minimizing the ratio between the reflected energy and the incident energy over a range of incident angles. For an isotropic medium, this results in

$$A_1 = \frac{8}{15\pi}(5 + 2S - 2S^2) \tag{32}$$

$$A_2 = \frac{8}{15\pi}(3 + 2S), \tag{33}$$

which gives slightly better over-all efficiency than the original approach [Lysmer and Kulhemeyer (1969)]. The value of S in Eq. (32) and Eq. (33) is given by

$$S = \sqrt{\frac{(1-2\nu)}{2(1-\nu)}}. \tag{34}$$

These local viscous dampers represent the exact solution for P- and S-waves, which impinge at a right angle on the artificial boundary. They are approximate for inclined body waves, whereby the reflected energy is only a small part of the total energy [Lysmer and Kuhlemeyer (1969)]. In many cases, the farther one chooses the artificial boundary to be from a source that radiates waves, the more the angle of incidence with respect to the artificial boundary will approach 90°C. In this way, the viscous dampers will perform better. The same applies as the frequency of excitation becomes higher.

6. Iterative Scheme for SSI Problems

The equations of motion for dam and foundation system are written separately as follows:

$$M_d\ddot{x}_d + C_d\dot{x}_d + K_d x_d = f_d \tag{35}$$

$$M_f\ddot{x}_f + C_f\dot{x}_f + K_f x_f = f_f + f_{if}. \tag{36}$$

Here, M, C, K, and f are the mass, damping, stiffness, and the applied load matrices. The suffixes d and f represent dam and foundation domain, respectively. The load vector f_d includes the hydrodynamic forces developed from reservoir water, the earthquake forces, self-weight of the dam body, and any other external forces if present. The vector f_{if} is the vector of interactive force for the soil region exerted by the dam body. The vector f_{if} is generated during successive iteration at the interface nodes of dam and foundation. The vectors of acceleration, velocity, and displacement for the dam part at any time step t are represented by $\ddot{x}_d, \dot{x}_d$, and x_d. The vectors $\ddot{x}_f, \dot{x}_f$, and x_f also carry similar meaning for the foundation part.

The damping matrix C has been assumed to be the Rayleigh damping matrix and is constructed as a linear combination of M and K matrices as follows:

$$C = \alpha M + \beta K. \tag{37}$$

The matrices M_d, M_s and K_d, K_s are built from the following formulae:

$$M_d = \int_{\Omega_d} [N_d]^T \rho_d [N_d] d\Omega_d \tag{38}$$

$$M_f = \int_{\Omega_f} [N_f]^T \rho_f [N_f] d\Omega_f \tag{39}$$

$$K_d = \int_{\Omega_d} [B_d]^T [D_d][B_d] d\Omega_d \tag{40}$$

$$K_f = \int_{\Omega_f} [B_f]^T [D_f][B_f] d\Omega_f, \tag{41}$$

where $[B_d], [B_f]$ are the strain displacement matrices and $[N_d], [N_f]$ are the matrices for the shape functions for dam and the soil foundation portions, respectively. Also $[D_d], [D_f]$ are the constitutive matrices and ρ_d, ρ_f represent the material densities for dam and foundation part, respectively.

The iterative scheme has been developed to determine the responses of the dam–foundation coupled system (Fig. 4). At any instant of time t, the equation of motion for the dam part (35) is solved first with the applied load f_d considering dam to be fixed at the bottom i.e. at the dam–foundation interface nodes. The exerted forces give rise to reaction forces at the common nodes of dam–foundation interface. The reaction forces generated at the common interface nodes of structure and foundation are then applied in the opposite direction at the common nodes of the foundation

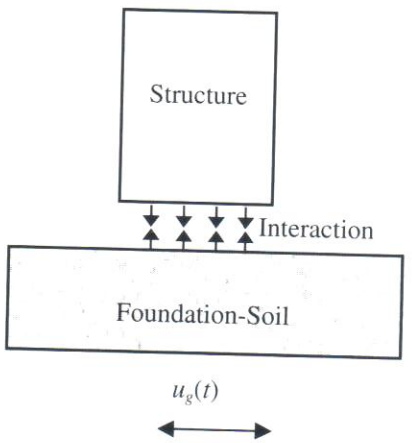

Fig. 4. Soil-structure interaction employed through reaction forces at the interface.

system to solve Eq. (36) at the same time instant t. These reaction forces applied in the opposite direction for the foundation part is termed as f_{if}.

After solving the foundation part against the applied load of $(f_f + f_{if})$, the common interface nodes for the foundation part will undergo some displacement. These displacements are then fed into Eq. (36) in the next instant of time $(t + \Delta t)$ or t_{i+1} as the known displacements at the common interface nodes. The iterations are continued for a particular time step t until the displacements and stresses for

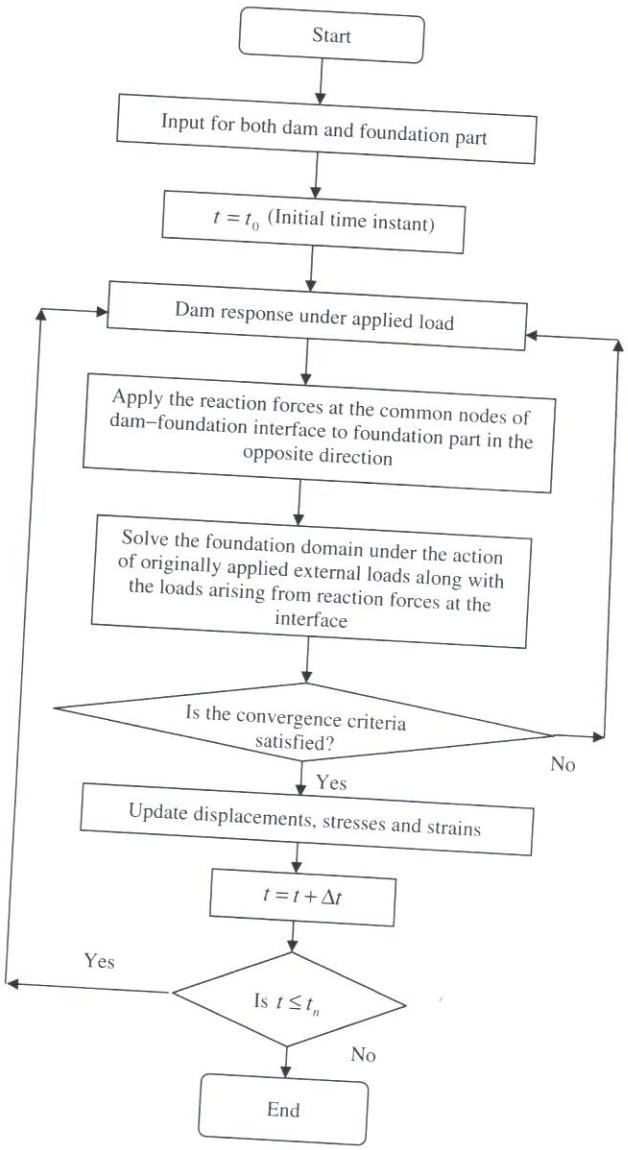

Fig. 5. Flowchart of the proposed algorithm for dam–foundation interaction analysis.

both the dam and foundation part are found to be converged with a certain level of tolerance. The iterations at a particular time step are stopped if the following relationships are satisfied:

$$\frac{|\{x_d\}_{i+1}^t - \{x_d\}_i^t|}{|\{x_d\}_i^t|} \leq \varepsilon \quad \text{and} \quad \frac{|\{x_f\}_{i+1}^t - \{x_f\}_i^t|}{|\{x_f\}_i^t|} \leq \varepsilon. \tag{42}$$

Here, i is the number of iteration, ε is a small pre-assigned tolerance value, and t is a particular time instant. The value of ε used in the present analysis is 0.01.

A flowchart of the iterative scheme for the solution method of coupled dam–foundation system is presented in Fig. 5. In the flowchart, t_0 and t_n stand for the initial and final time instants, respectively. The term Δt represents the time step of the Newmark's method. The most costly operation involved in the above algorithm is to solve successively two separate systems of equations at each iteration. However, in the present case, matrices involved in the solution of the system equations are decomposed into triangular forms at the beginning of the of the iteration, and thereby only two forward eliminations and backward substitutions are required at each iteration step. Thus, the required time is minimized to obtain the coupled response for a particular time instant.

7. Numerical Results and Discussions

7.1. *Validation of the proposed algorithm*

In order to validate the proposed algorithm, a concrete gravity dam–foundation prototype resting on rock foundation is analyzed. The same dam–foundation interaction problem has been previously analyzed by Yazdchi *et al.* [1999]. While solving the dam–foundation interaction problem, the side nodes of the discretized finite elements in the foundation portions were considered to be rollers allowing only the horizontal movements and the bottom nodes were kept fixed. The dam and the foundation domain has been discretized using 2D, plane strain, and isoparametric finite elements. A 2×2 Gauss integration rule is adopted for the calculation of both the stiffness matrix and the mass matrix. The dimensions of the dam prototype are depicted in Fig. 4. The width of the base of the dam is 10.0 m. The height of the dam is 15.0 m out of which the crest portion is of 6.0 m in length. The width of the crest is considered as 2.0 m. The width and the depth of the foundation part are considered as 100.0 m and 50.0 m, respectively. The width and height of the foundation domain considered for the analysis purpose are the same as those considered by Yazdchi *et al.* [1999]. The material properties of the dam and the foundation part are taken same and are as follows:

The Young's modulus: 30.0 GPa
The Poisson's ratio: 0.20
The mass density: 2600.0 kg/m^3.

7.2. *Selection of an optimum mesh size*

To check the convergence of the results obtained for various mesh grading, a simplified section of the dam prototype [solved by Yazdchi *et al.* (1999)] has been chosen for the extensive analysis using finite element technique. The slope on the downstream face above the neck of the dam is also neglected in the present analysis. The dimension and the material properties of the dam in the present case are same as listed before. The dam is discretized with eight-noded quadratic elements as shown in Fig. 6 and is analyzed using plain strain formulation. In order to arrive at suitable mesh gradation for dam prototype used by Yazdchi *et al.* [1999], a unit ramp acceleration is applied on the body of the dam. For different mesh grading, the horizontal crest displacement observed at the rightmost crest point (as shown by point "O" in Fig. 6) is plotted in Fig. 7. It is observed from the results that the solution converges sufficiently for a discretization of 7×4 (vertical $\times$ horizontal). However, a higher mesh grading 10×4 is adopted for the analysis for the sake of increased accuracy.

For the foundation domain also, similar convergence analyses for mesh grading were carried out. In order to fix the mesh division of the foundation domain, unit ramp acceleration is applied throughout the body of foundation. The horizontal displacement at the middle node on the top of the foundation domain is plotted in Fig. 8 for different mesh grading. The width and the depth of the foundation part are considered to be 100.0 m and 50.0 m, respectively. The bottom nodes were

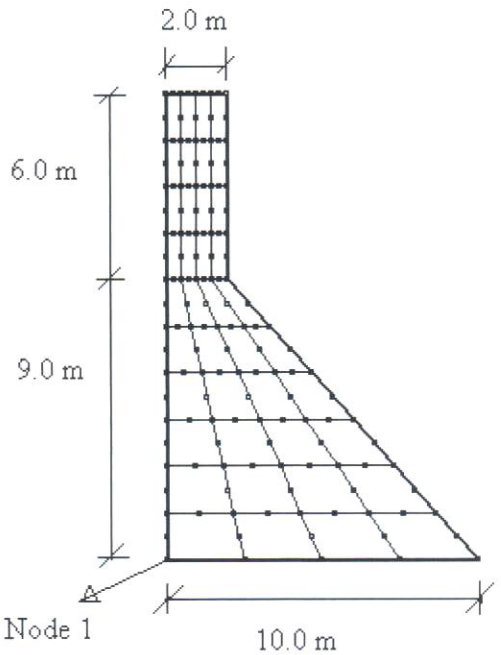

Fig. 6. The geometry of dam [Yazdchi *et al.* (1999)].

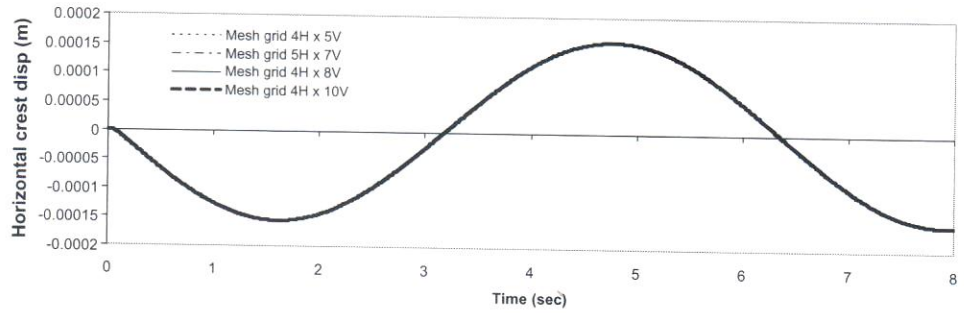

Fig. 7. Convergence of horizontal crest displacement for dam prototype [Yazdchi *et al.* (1999)] for different mesh division.

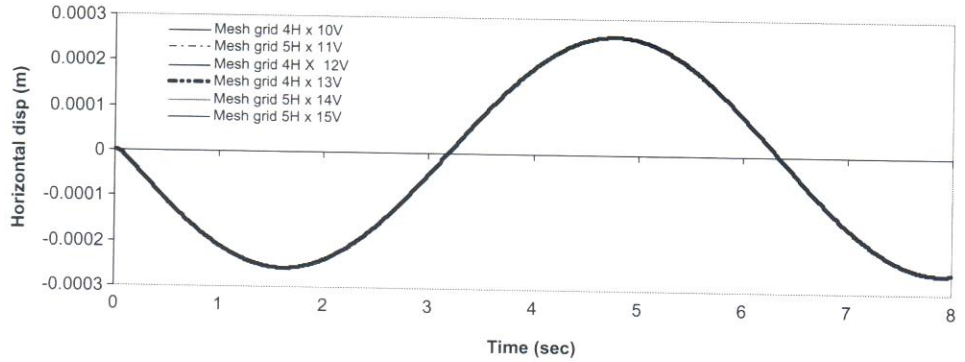

Fig. 8. Convergence of horizontal displacement at the mid-point of the surface of foundation for dam prototype [Yazdchi *et al.* (1999)] for different mesh division.

considered to be fixed in both directions. The side nodes at the truncated boundary were considered to be rollers allowing horizontal movements. The dashpots were modeled as described in Sec. 5. The time periods and the displacements of the point where the load is applied have been tabulated in Table 2. It is observed that the result converges for a mesh grading of 12×4.

7.3. *Comparison of the results of the proposed model with published results*

Having arrived at a suitable mesh grading for both the dam and the foundation domain, an attempt is made to compare our results with the dam–foundation interaction problem solved by Yazdchi *et al.* [1999]. While doing so, suitable boundary conditions were applied at the truncated boundaries as well as at the bottom of the foundation domain and all the concerned nodes were fitted with dashpots. The Koyna earthquake acceleration is applied to the dam prototype with a scaling factor

of 2.5. This factor has been used by Yazdchi *et al.* [1999] while applying the Koyna earthquake acceleration to the dam prototype. Therefore, in the present work also, this factor has been used while validating the developed computer program for dam–foundation interaction analysis. The earthquake acceleration data is presented in Fig. 9. Yazdchi *et al.* [1999] solved this problem by the coupled FEM–BEM method. They included the effect of viscous damping with a damping ratio of 0.05. Moreover, the effect of hydrodynamic pressure is incorporated in the analysis by the added mass concept proposed by Westergaard [1933]. The effect of wave scattering and reflection was tackled by coupled FEM–BEM method. When the same dam–foundation model is solved by the proposed iterative scheme in this paper, the effect of viscous damping and the hydrodynamic pressure is also considered in similar way. Moreover, initially the dam has been analyzed considering the effects of its self-weight and the hydrostatic pressure, which produced initial acceleration in the dam body. The horizontal extent of the foundation portion is arbitrarily truncated at a certain distance from both the upstream and the downstream face of the dam. The value of tolerance ε used in Eq. (45) is 0.01. In addition, the time interval used for solution of dynamic equilibrium equations (38) and (39) is 0.01 second.

Different boundary conditions were tested on the dam–foundation coupled model. First, the side boundary nodes are fully kept fixed as shown in Fig. 10(a). Then, these nodes are released and fitted with dashpots in both normal and tangential directions. The perpendicular dashpots to the boundary absorb the P-waves, whereas the dashpots tangential to the boundary absorb the S-waves. In these models, no displacement constraints are used. Preisig [2002] suggested that the horizontal at rest earth pressure be applied at the boundary nodes situated at the both sides of the foundation domain. This is done by recording the reaction forces in the model with fixed boundaries and applying them with opposite sign to the model with absorbing boundaries.

This configuration of boundary conditions has no fixed point in x-direction. Because the dashpots only provide resistance to high-velocity motions the model is very sensitive to low-frequency components of the motion. The slightest imbalance

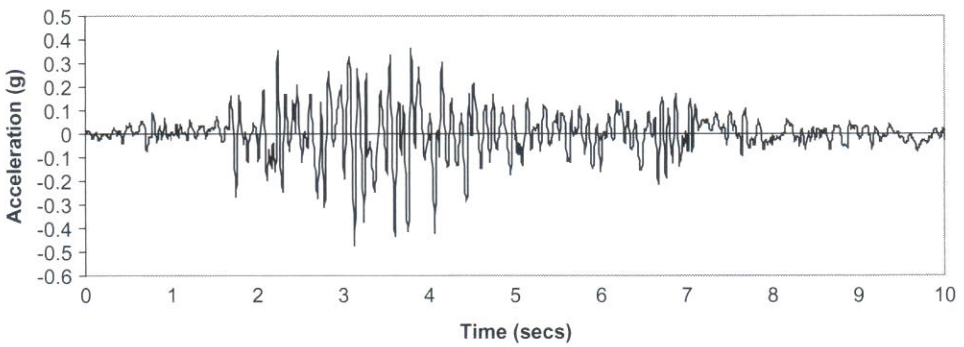

Fig. 9. Koyna earthquake acceleration data.

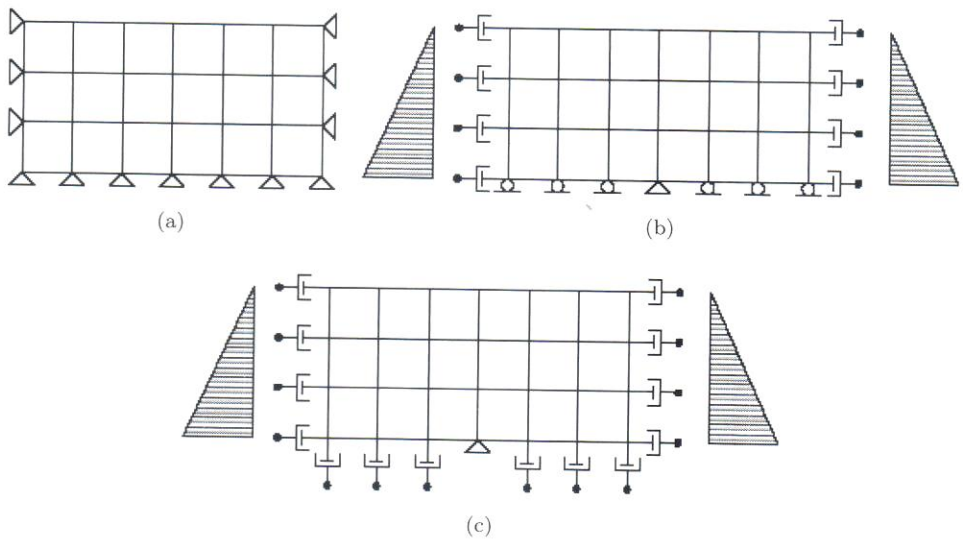

Fig. 10. Boundary conditions for 2D model.

in acceleration causes the entire model to move as a rigid body in x-direction [Preisig (2002)]. To avoid this, the node at the center of the base is fully fixed in the following analyses. Keeping the center node at the base of the foundation as fixed, two varieties of boundary conditions were tested. First, all the bottom nodes were provided with rollers allowing only horizontal movements as shown in Fig. 10(b) and second, the boundary nodes at the bottom of the base were fitted with dashpots as shown in Fig. 10(c). However, in both these cases, the side nodes of the foundation domains were attached to dashpots in both normal and tangential directions. A detailed description of the use of dashpots can be found in the works by Preisig [2002].

The nodes at the truncated boundary as well as at the bottom are provided with dashpots in both the horizontal and tangential directions. In spite of these anomalies with the original solution by Yazdchi *et al.* [1999], the proposed model yields a similar displacement pattern of the horizontal displacement at the crest node though the magnitudes differed. In the present work, the hydrodynamic pressures at the upstream face of the dam are calculated from Eq. (24). These hydrodynamic forces are applied on the upstream face of the dam. Table 1 shows the comparison between the results of Yazdchi *et al.* [1999] and that of the proposed method for different E_f/E_d (impedance ratio) ratios. The maximum crest displacement of the dam under seismic excitation by both the methods has been tabulated in the Table 1 for a comparison purpose. The obtained displacements by the proposed interaction scheme are in very close agreement with the results obtained by Yazdchi *et al.* [1999]. The slight discrepancy between the two results might be due to (i) use of different methods and numerical tools for the solution of the coupled system and (ii) different mesh sizes considered for the problem. Moreover, it is observed that

Table 1. Comparison of maximum horizontal crest displacements.

Horizontal crest displacements (mm)		Coupled FE–BE solution [Yazdchi *et al.* (1999)]	Staggered method with boundary conditions as per Fig. 10(b)	Percentage of deviation	Staggered method with boundary conditions as per Fig. 10(c)	Percentage of deviation
Impedance ratio (E_f/E_d)	0.5	6.89	6.99	1.45	7.14	3.63
		−7.53	−7.20	4.38	−7.38	1.99
	1.0	4.38	4.72	7.76	4.94	12.79
		−4.41	−4.28	2.95	−4.69	6.35
	2.0	4.27	4.11	3.74	4.36	2.11
		−3.85	−3.97	3.12	−3.99	3.64
	4.0	4.11	3.90	5.11	3.95	3.89
		−3.70	−3.57	3.51	−3.47	6.22

the results from the model where bottom nodes were provided with rollers are closer to that of Yazdchi *et al.* [1999] compared to the results obtained from the model where the bottom nodes are also attached to dashpots. Therefore, in subsequent calculations, the bottom nodes of the foundation domain were provided with rollers except the center node that will remain to be fully fixed to prevent any type of rigid body translation.

The use of dashpots as a viscous boundary to absorb the traveling earthquake waves serve as a simple and effective approach in dealing with semi-infinite foundation domain. But, one should be cautious while using them because they are local in nature. They should be placed far away from the source of originating waves. On the other hand, the boundary element method used by Yazdchi *et al.* [1999] satisfies the radiation boundary condition satisfies automatically. If the nonlinearity of the foundation material is to be considered in the analysis, then the use of boundary element method would become difficult since it is more suited to linear analysis. In addition, the mathematical complexities involved with boundary element method makes it unattractive from the user's viewpoint. The implementation of dashpots at the foundation boundary allows us to use finite element method exclusively for the entire dam and foundation domain, which is a much simpler method than the boundary element method. In addition, finite element methods are more efficient in modeling nonlinear behavior of the material than the boundary element method.

7.4. *Response of Koyna dam*

The seismic response of Koyna dam has been investigated considering the interaction behavior of a linear and elastic concrete dam and foundation subjected to Koyna earthquake [1967] acceleration. The foundation material is assumed to be of hard rock. The width and the depth of the foundation are assumed to be 250.0 m and 100.0 m, respectively. The geometry of the dam–foundation system chosen for the analysis purpose is shown in Fig. 11. The material properties of the dam are as follows.

The Young's modulus of dam body is assumed to be 3.15 GPa. The Poisson's ratio is taken to be 0.20, and the mass density is assumed as $2415.816\,\mathrm{kg/m^3}$.

The Young's modulus of foundation rock is considered to be 1.75 GPa. The Poisson's ratio is assumed as 0.2. The mass density of the foundation material is assumed to be $1800.0\,\mathrm{kg/m^3}$.

In order to arrive at an optimum mesh grading for this particular problem, the response of the dam and the foundation domain under the action of a given load is found out. For the dam part, unit ramp acceleration is applied horizontally and the horizontal displacement of the crest node is observed. It is observed that the results converged sufficiently for a mesh grading of 8×5. Similarly, for the foundation domain, unit ramp acceleration is applied on the foundation domain and convergence of the horizontal displacement at the middle node on the surface

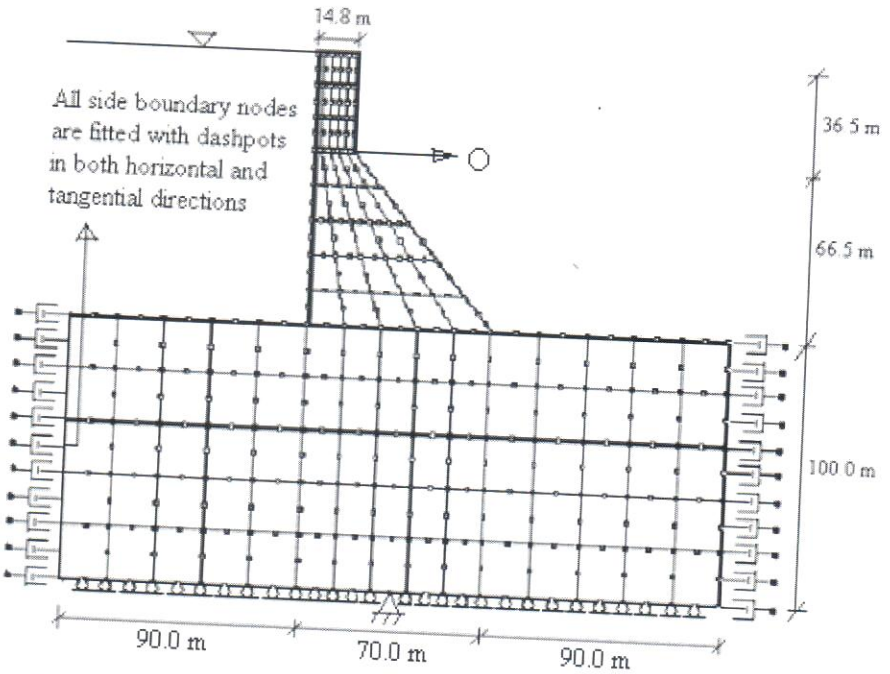

Fig. 11. The geometry and boundary condition of the Koyna dam–foundation system.

of the foundation is studied. It is observed that the results converged for a mesh size of 15×5 with sufficient degree of accuracy. However, the results for this analysis are not provided here, as they are similar in nature with those of the previous analysis of dam–foundation prototype solved by Yazdchi *et al.* [1999].

7.4.1. *Evaluation of degradation index*

Next, the variation of degraded elastic modulus with age is observed. The elastic modulus of concrete (E_0) considering the strength gain with age is obtained from Eq. (22). Having obtained the value of E_0, the degraded elastic modulus E_n is calculated from Eq. (6). The variation of elastic modulus of concrete considering hygrochemomechanical effects with design life of 100 years is plotted in Fig. 12. The degraded elastic modulus is found out as a function of the elastic modulus, which is expressed in terms of compressive strength of concrete at a certain age as expressed by Eq. (21). In Fig. 12, the variation of the degraded elastic modulus with the material parameter a_s is also plotted. In case of hygrochemomechnically induced degradation, the total porosity, ϕ, of concrete is expressed as the summation of initial porosity, ϕ_0, chemically induced porosity, ϕ_c, and mechanically induced porosity, ϕ_m, according to Eq. (6). The values of ϕ_0 is considered to be 0.2 [Gogoi and Maity (2007); Kuhl *et al.* (2004)]. Following Eq. (7), the value of mechanically induced porosity, ϕ_m, is expressed as a function of scalar degradation parameter, d_m,

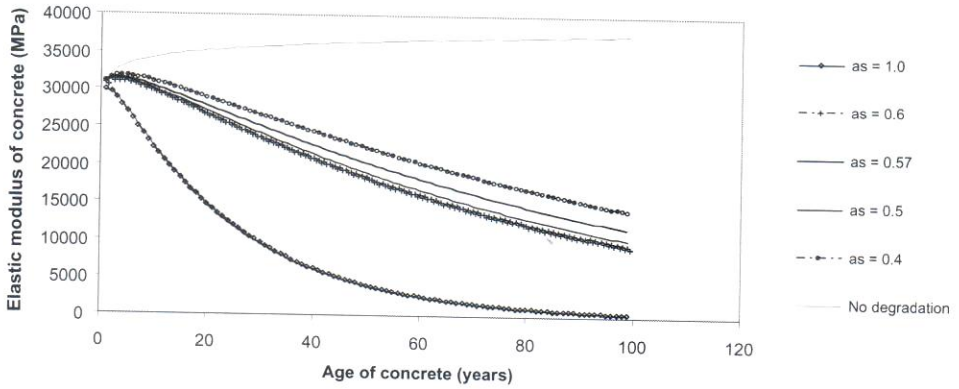

Fig. 12. Variation of elastic modulus of concrete with age (design life = 100 years).

which may be calculated from Eq. (8). In Eq. (8), the values of material parameters $\alpha_m, \beta_m, \phi_0$ and κ^0, are considered to be 0.9, 1000, 0.2, and 1.1×10^{-4}, respectively [Kuhl *et al.* (2004)]. The value of ϕ_c may be considered between 0.0 and 0.2 in the presence of chemical degradation due to silt deposition on the upstream face of the dam. The maximum allowable range of values for d_m should lie between 1.0 and 0.0 indicating complete and no degradation of concrete, respectively. The value of the material parameter a_s has been varied from 0.4 to 1.0 for an HCM (hygrochemomechanical) design life of 100 years. The variation of elastic modulus with different values a_s has been plotted in Fig. 12. The elastic modulus has been calculated by using Eq. (21). It is observed that considering $a_s = 1.0$ reduces the value of elastic modulus of concrete to a very low value that is practically incorrect. Having observed the effects of the different values of the material parameter a_s, the value of has been fixed at 0.57 for further analyses.

7.4.2. *Response of aged Koyna dam with dam–foundation interaction*

The dam–foundation interaction effect is observed for aged Koyna dam. The material properties of the dam and foundation domain are same as stated in Sec. 7.4. In order to simulate the infinite foundation domain, viscous dashpots are provided at the nodes of the truncated boundary. The geometry and the boundary conditions are shown in Fig. 11.

The effect of HCM design life on the response of dam–foundation interaction analyses has been studied next. The foundation material is assumed to follow a linear and elastic behavior. The HCM design life of the concrete of the dam region is altered and the interaction analyses were carried out at the end of 25 years after construction of the structure. Figure 13 shows the comparison of horizontal crest displacement under earthquake loading for HCM design lives of 50 years and 100 years, respectively. It is observed that the horizontal crest displacement reduces if the design life of the dam structure is considered more. For a design life of 50

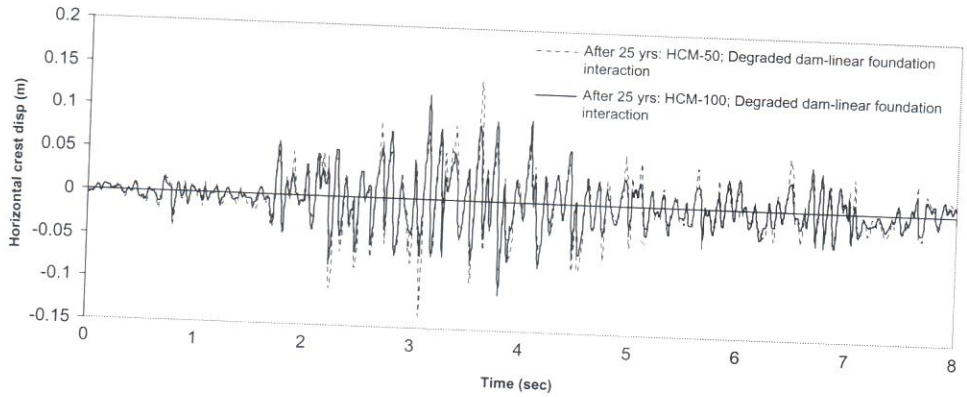

Fig. 13. Comparison of horizontal crest displacement between degraded dam–linear foundation interaction after 25 years of construction for different HCM design lives.

years, the maximum and minimum values of the horizontal crest displacements were found out to be 13.8 cm and −13.3 cm, respectively. For a design life of 100 years, the same quantities were found out to be 12.1 cm and −10.90 cm, respectively. Therefore, the maximum and minimum values of the horizontal crest displacements reduces by 12.3% and 18.0%, respectively if the design life of the concrete of the dam region is increased from 50 years to 100 years.

Figure 14 plots the variation of major principal stress vs. time at the neck region (point "O" as seen in Fig. 11) for dam–linear foundation interaction analyses at the end of 25 years after construction for different values of HCM design life. If the deign life is considered to be 50 years, the maximum major principal stress is found out to be 11.50 MPa, whereas the maximum major principal stress is obtained as 14.44 MPa when the HCM deign life is increased to 100 years. Therefore, it is observed that consideration of higher design life yields more stress compared to the case when design life is reduced. A reduction of 20.36% takes place when the design life is reduced to 50 years from 100 years. With lower design life, the degradation

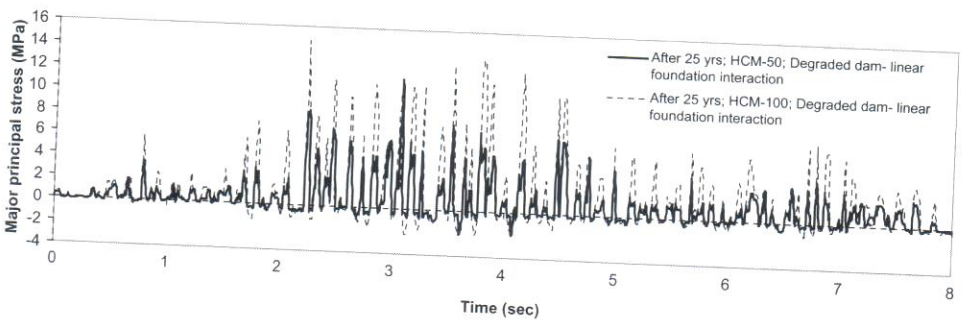

Fig. 14. Major principal stress vs. time at the neck from degraded dam–linear foundation interaction after 25 years of construction with different HCM design lives.

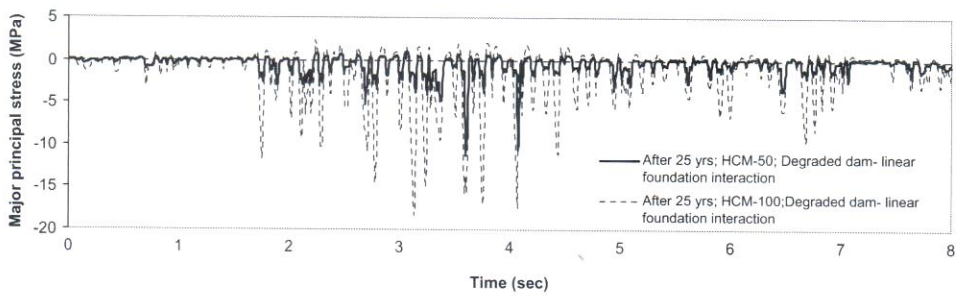

Fig. 15. Minor principal stress vs. time at the neck from degraded dam–linear foundation interaction after 25 years of construction with different HCM design lives.

index obtained is more, which in turn reduces the constitutive matrix ($[D]$) of the material. In addition, at a later stage of the material, the loss of stiffness is also higher due to higher value of degradation index. For this reason, less stresses may be obtained even though more displacements occur in the analyses with lower design life. Since, the generated stress $\{\sigma\}$ is equal to $[D][B]\{u\}$, the comparative severity between the decrement of the $[D]$ matrix and the increment of $\{u\}$ vector will actually determine whether the generated stress will be more or less. However, in this case, higher stresses are obtained when the design life is 100 years compared to the design life of 100 years. Therefore, in this case, the decrement in $[D]$ matrix due to consideration of lower design life is more predominant than the increase in $\{u\}$ vector. Similarly, Fig. 15 plots the distribution of minor principal stresses with respect to time at the neck node "O" for dam–foundation interaction analyses with HCM design life of 50 years and 100 years. With design life of 100 years, the minimum value of the minor principal stress is obtained as -18.39 MPa and with design life of 50 years; the minimum value of minor principal stress is obtained as -11.11 MPa. Therefore, a reduction of 39.6% in the values of minor principal stress occurs if the design life is reduced to 50 years from 100 years. Here also, while changing the design life from 100 years to 50 years, the reduction in $[D]$ matrix for consideration of lower design life governs the relative increase or decrease in the value of generated stresses.

8. Conclusions

The present paper illustrates a simple but efficient iterative method for the dynamic analysis of soil–structure interaction problems. The proposed algorithm of soil–structure interaction is quite simple and can be programmed with ease. Here, the two individual systems are solved separately and the interaction effects are incorporated through an iterative manner at the interface level. The accuracy of the developed algorithm is validated with the published literature. The Koyna dam–foundation system is solved under Koyna earthquake acceleration. The effect of hydrodynamic pressure on the dam has also been included in the dynamic analysis

of dam–foundation coupled system. In order to consider the semi-infinite nature of the foundation domain, viscously damped dashpots is employed effectively at the boundary of the soil domain. The parametric study reveals that the dam produces more displacements with its age. Furthermore, the design life of concrete bears a significant effect on the response of dam–foundation interaction analysis. It is observed that the degradation of the concrete is less if the design life of concrete is considered higher and vice versa. If the HCM design life is less, the amount of degradation is more, which leads to excessive loss of stiffness of the material. This loss of stiffness of the material may reduce the stress experienced by the structure but it normally increases the displacement of the structure. An accurate seismic behavior of a dam–foundation system can be predicted at any age by the proposed interaction analysis procedure that would assist designers to take appropriate measure at the beginning itself.

References

Atkin, P. W. [1994] *Physical Chemistry*, Fifth Edition, Oxford University Press, Oxford, U.K.

Bangert, F., Grasberger, S., Kuhl, D. and Meschke, G. [2003] Environmentally induced deterioration of concrete: Physical motivation and numerical modelling, *Eng. Fract. Mech.* **70**, 891–910.

Bazant, Z. P. and Xiang, Y. [1997] Crack growth and lifetime of concrete under long time loading, *J. Eng. Mech. ASCE* **123**(4), 350–358.

Bazant, Z. P., Hauggaard, A. B., Baweja, S. and Ulm, F. J. [1997] Microprestress-solidification theory for concrete creep. I: Aging and drying effects, *J. Eng. Mech. ASCE* **123**(11), 1188–1194.

Cervera, M., Oliver, J. and Prato, T. [1999a] Thermo-chemo-mechanical model for concrete. I: Hydration and aging, *J. Eng. Mech. ASCE* **125**, 1018–1027.

Cervera, M., Oliver, J. and Prato, T. [1999b] Thermo-chemo-mechanical model for concrete. II: Damage and creep, *J. Eng. Mech., ASCE*, **125**, 1028–1039.

Cervera, M., Oliver, J. and Prato, T. [2000a] Simulation of construction of RCC dams I: Temperature and aging, *J. Struct. Eng. ASCE* **126**(9), 1053–1061.

Cervera, M., Oliver, J. and Prato, T. [2000b] Simulation of construction of RCC dams. II: Stress and Damage, *J. Struct. Eng. ASCE* **126**(9), 1062–1069.

Chopra, A. K. and Chakrabarty, P. [1981] Earthquake analysis of concrete gravity dams including dam-fluid-foundation rock interaction, *Earthquake Eng. Struct. Dyn.* **9**, 363–383.

Estorff, O. V. and Kausel, E. [1989] Coupling of boundary and finite elements for soil–structure interaction problems, *Earthquake Eng. Struct. Dyn.* **18**, 1065–1075.

Estorff, O. V. and Hagen, C. [2005] Iterative coupling of FEM and BEM in 3D elastodynamics, *Eng. Anal. Bound. Elem.* **29**, 775–787.

Felippa, C. A. and Park, K. C. [1980] Staggered transient analysis procedures for coupled mechanical systems: Formulation, *Comput. Methods Appl. Mech. Eng.* **24**, 61–111.

Fenves, G. and Chopra, A. K. [1985] Simplified earthquake analysis of concrete gravity dams: Separate hydrodynamic and foundation effects, *J. Eng. Mech. ASCE* **111**(6), 715–735.

Ghaemian, M. and Ghobarah, A. [1999] Nonlinear seismic response of concrete gravity dams with dam-reservoir interaction, *Eng. Struct.* **21**, 306–315.

Ghrib, F. and Tinawi, R. [1995] An application of damage mechanics for seismic analysis of concrete gravity dams, *Earthquake Eng. Struct. Dyn.* **24**(2), 157–173.

Gogoi, I. and Maity, D. [2007] Influence of sediment layers on dynamic behavior of aged concrete dams, *J. Eng. Mech. ASCE* **133**(4), 400–413.

Grote, M. J. and Keller, J. B. [1996] Nonreflecting boundary conditions for the time scattering, *J. Comput. Phys.* **127**, 52–65.

Jahromi, H. Z., Izzuddin, B. A. and Zdravkovic, L. [2007] Partitioned analysis of nonlinear soil–structure interaction using iterative coupling, *Interact. Multiscale Mech.* **1**(1), 33–51.

Kuhl, D., Bangert, F. and Meschke, G. [2004] Coupled chemo-mechanical deterioration of cementitious materials. Part I: Modeling, *Int. J. Solids Struct.* **41**, 15–40.

Lysmer, J. and Kuhlemeyer, R. L. [1969] Finite dynamic model for infinite media, *J. Eng. Mech. Divi. ASCE* **95** (EM4), 859–877.

Maity, D. and Bhattacharyya, S. K. [2003] A parametric study on fluid structure interaction problems, *J. Sound Vib.* **263**, 917–935.

Mathews, J. H. [2001] *Numerical Methods for Mathematics, Science and Engineering*, Prentice-Hall of India, New Delhi, pp. 257–314.

Meschke, G. and Grasberger, S. [2003] Numerical modeling of coupled hygromechanical degradation of cementitious materials, *J. Eng. Mech. ASCE* **129**(4), 1–10.

Neville, A. M. and Brooks, J. J. [1987] *Concrete Technology*, Pearson Education (Singapore) Pte. Ltd., Fourth Indian Reprint, pp. 209–234.

Preisig, M. [2002] Nonlinear finite element analysis of dynamic soil–foundation–structure interaction, Dissertation submitted for Master of Science in Civil Engineering, University of California, Davis. Swiss Federal Institute of Technology, Lausanne.

Rizos, D. C. and Wang, Z. [2002] Coupled BEM–FEM solutions for direct time domain soil–structure interaction analysis, *Eng. Anal. Bound. Elem.* **26**, 877–888.

Steffens, A., Li, K. and Coussy, O. [2003] Ageing approach to water effect on alkali–silica reaction degradation of structures, *J. Eng. Mech. ASCE* **129**(1), 50–59.

Simo, J. and Ju, J. [1987] Strain and stress-based continuum damage models — I. Formulation, *Int. J. Solids Struct.* **23**(7), 821–840.

Thompson, L. L. and Huan, R. N. [2000] Implementation of exact non-reflecting boundary conditions in the finite element method for the time dependent wave equation, *Comput. Methods Appl. Mech. Eng.* **187**, 137–159.

Ulm, F. J. and Coussy, O. [1995] Modelling of thermochemomechanical couplings of concrete at early ages, *J. Eng. Mech. ASCE* **121**(7), 785–794.

Washa, G. W., Saemann, J. C. and Cramer, S. M. [1989] Fifty year properties of concrete made in 1937, *ACI Mater. J.* **86**(4), 367–371.

Westergaard, H. M. [1933] Water pressures on dams during earthquakes, *Trans. ASCE* **98**, 418–472.

White, W., Valliappan, S. and Lee, I. K. [1977] Unified boundary for finite dynamic models, *J. Eng. Mech. Div. ASCE* **103**, 949–964.

Wolf, J. P. [1985] *Dynamic Soil–Structure Interaction*, Prentice Hall, Englewood Cliffs, New York.

Wolf, J. P. and Song, C. [1996] *Finite Element Modeling of Unbounded Media*, Wiley, New York.

Yazdchi, M., Khalili, N. and Valliappan, S. [1999] Dynamic soil–structure interaction analysis via coupled finite element-boundary element method, *Soil Dyn. Earthquake Eng.* **18**, 499–517.

Zienkiewicz, O. C., Kelly, D. W. and Bettes, P. [1977] The coupling of the finite element methods and boundary solution procedures, *Int. J. Num. Meth. Eng.* **11**, 355–377.